SHORT-ROOT Stabilizes PHOSPHATE1 to Regulate Phosphate Allocation in Arabidopsis

Xinlong Xiao
Center for Excellence in Molecular Plant Sciences
Jieqiong Zhang
CAS Center for Excellence in Molecular Plant Sciences
Viswanathan Satheesh
CAS Center for Excellence in Molecular Plant Sciences
Fanxiao Meng
CAS Center for Excellence in Molecular Plant Sciences
Wenlan Gao
CAS Center for Excellence in Molecular Plant Sciences
Jinsong Dong
Shanghai Center for Plant Stress Biology and Center for Excellence in Molecular Plant Sciences, Chinese Academy of Sciences, Shanghai https://orcid.org/0000-0001-9861-1851
Zai Zheng
Tsinghua University https://orcid.org/0000-0001-5773-9402
Guoyong An
Laboratory of Plant Stress Biology, Department of Biology, Henan University, Kaifeng 475001, China
Laurent Nussaume
(CEA)Commissariat à l'Energie Atomique et aux Energies Alternatives https://orcid.org/0000-0002-9445-2563
Dong Liu
Tsinghua University https://orcid.org/0000-0002-4679-3515
Mingguang Lei (mglei@cemps.ac.cn)
CAS Center for Excellence in Molecular Plant Sciences https://orcid.org/0000-0002-6431-4530

Letter

Keywords: Arabidopsis SHORT-ROOT, PHO1, PHB, PHO2, Pi allocation

Posted Date: January 14th, 2022

DOI: https://doi.org/10.21203/rs.3.rs-1169316/v1

Version of Record: A version of this preprint was published at Nature Plants on September 1st, 2022. See the published version at https://doi.org/10.1038/s41477-022-01231-w.

Title: SHORT-ROOT Stabilizes PHOSPHATE1 to Regulate Phosphate Allocation in *Arabidopsis*

Authors/Affiliations

Xinlong Xiao[1#], Jieqiong Zhang[1,2,3#], Viswanathan Satheesh[1], Fanxiao Meng[1,3], Wenlan Gao[1,3], Jinsong Dong[1], Zai Zheng[4], Guo-Yong An[5], Laurent Nussaume[6], Dong Liu[4], and Mingguang Lei[1,5*]

1. Shanghai Center for Plant Stress Biology, CAS Center for Excellence in Molecular Plant Sciences, Chinese Academy of Sciences, Shanghai, 200032, China

2. School of Life Science and Technology, Tongji University, Shanghai, 200092, China

3. University of Chinese Academy of Sciences, Beijing, 100049, China

4. School of Life Sciences, Tsinghua University, Beijing, 100086, China

5. Key Laboratory of Plant Stress Biology, School of Life Sciences, Henan University, Kaifeng 475004, China

6. Laboratoire de Biologie du Développement des Plantes, Commissariat à l'Énergie Atomique et aux Énergies Alternatives, UMR7265 (CEA, Aix-Marseille Université, CNRS), Saint Paul-Lez-Durance, F-13108, France.

#. These authors contributed equally to this article.

Corresponding author:

Mingguang Lei (mglei@cemps.ac.cn)

Running Title:

SHR regulates Pi homeostasis in *Arabidopsis*

Abstract

Coordinated distribution of Pi between roots and shoots is an important process that plants use to maintain Pi homeostasis. SHR (SHORT-ROOT) is well-characterized for its function in root radial patterning[1-3]. Here, we demonstrate a new role of SHR in controlling phosphate (Pi) allocation from roots to shoots by regulating PHOSPHATE1 (PHO1) in the root differentiation zone. We recovered a weak mutant allele of *SHR* in *Arabidopsis* which accumulates much less Pi in the shoot and shows constitutive Pi starvation response (PSR) under Pi-sufficient condition. Besides, Pi starvation suppresses SHR protein accumulation and releases its inhibition on the HD-ZIP III transcription factor PHB. PHB accumulates and directly binds the promoter of *PHO2* to upregulate its transcription, resulting in PHO1 degradation in the xylem-pole pericycle cells. Our findings reveal a previously unrecognized mechanism of how plants repress Pi translocation from roots to shoots in response to Pi starvation.

Keywords: Arabidopsis SHORT-ROOT, PHO1, PHB, PHO2, Pi allocation

Main

As sessile organisms, plants have to orchestrate the uptake, usage and redistribution of Pi to maintain its homeostasis[4]. Under Pi deficiency condition, shoot growth is inhibited and more resource is allocated to the root to promote its growth to forage Pi from poor soil. PHO1 is specifically expressed in the root pericycle and critical for Pi loading into the xylem and transport to the shoot. However, previous studies indicate PHO1 was positively regulated by Pi deficiency both at the transcriptional and post-translational levels to promote Pi translocation from roots to shoots[5-8], which contradicts findings that show higher proportion of Pi and biomass being allocated to root when Pi was limited[9,10] (Supplementary Fig. 1). The underlying molecular mechanism that represses Pi allocation from roots to shoots under Pi starvation was unknown. Here, we show that Pi starvation inhibits Pi allocation to the shoot by repressing SHR in the root differentiation zone. Repression of SHR releases the transcription factor PHB, which directly activates PHO2 resulting in PHO1 degradation in the xylem pole pericycle cells.

To identify new cellular factors required for maintaining Pi homeostasis, we performed a forward genetic screen in *Arabidopsis* using *pPHT1;4::LUC* as the reporter gene[11]. In this report, we characterized a mutant, *phod1* (*pho*sphate *d*eficiency*1*), in which *pPHT1;4::LUC* was constitutively induced on Pi-replete medium (Fig. 1a and Supplementary Fig. 2a). To confirm that the induction of *pPHT1;4::LUC* in *phod1* was caused by the mutation of a regulatory component, we introduced the *phod1* mutation into a *pPHT1;4::GUS* reporter line by a genetic cross. Consistent with the *LUC*

61 expression pattern, the *pPHT1;4::GUS* activity was also enhanced by the *phod1*
62 mutation (Supplementary Fig. 2e). Furthermore, the endogenous *PHT1;4* transcript
63 level was also increased in the *phod1* mutant in the shoot and root by 5- and 3-fold,
64 respectively (Fig. 1b).
65 To identify the causative mutation for the constitutive activation of *PHT1;4*, *phod1* was
66 backcrossed, and the genomic DNA from the pooled F_2 seedling with increased LUC
67 signal was deep sequenced (Supplementary Fig. 2a-c). The data were analyzed
68 following a mapping-by-sequencing workflow[12]. In the *phod1* mutant, a point mutation
69 (C866T) changes Thr-289 to Ile in *SHR* (Supplementary Fig. 2d). To confirm that the
70 increased expression of *PHT1;4* in the mutant is due to the mutation in the *SHR gene*,
71 we complemented the *phod1* mutant by *SHR* genomic DNA fragment fused to GFP or
72 FLAG driven by its native promoter (Fig. 1a,b and Supplementary Fig. 3a,b).
73
74 Loss-of-function of *SHR* severely inhibits root growth[1]. However, the T289I mutation
75 in *phod1* only weakly affected root growth. Although *phod1* primary root length was
76 shorter than WT, it was much longer than the knock-out line *shr-6* (Supplementary Fig.
77 4a). Unlike the *shr-6* null mutant, which has a disorganized root stem cell niche and
78 lacks the endodermis, the root meristem of *phod1* is relatively well-organized, and the
79 endodermal layer is present (Supplementary Fig. 4b). This result indicated that *phod1*
80 is a weak allele of *SHR*. To confirm this, we transformed the GFP-fused wild-type
81 (*SHR-GFP*) or *phod1* allele of *SHR* (*SHR*^{phod1}-GFP) driven by its native promoter into
82 the *shr-6* null mutant. The *shr-6 SHR*^{phod1} resulting transformant could mimic *phod1*

mutant phenotype (Supplementary Fig. 4a,h-i). Although their mRNA levels were comparable (Supplementary Fig. 4c,d), Western-blot analysis showed that the protein abundance of SHR^{phod1}-GFP was much lower than SHR-GFP (Supplementary Fig. 4e). Whereas the GFP signal detected in the vascular tissue and nucleus of endodermis and quiescent cells in *SHR-GFP* lines was strong, it was much weaker and barely detectable in the endodermis and quiescent cells of the *SHR^{phod1}-GFP* lines (Supplementary Fig. 4f). Furthermore, although SHR accumulation was not affected, SHR^{phod1} was enhanced by MG132 treatment, a 26S proteasome inhibitor, suggesting that SHR^{phod1} is prone to degradation by the 26S proteasome (Supplementary Fig. 4g). These results, therefore, further affirm that *phod1* is a weak allele of *SHR* and that Thr-289 is required for SHR protein stability.

Besides altered *PHT1;4* expression, the *phod1* mutant also exhibited constitutive PSR phenotypes under Pi-replete condition. The shoots of *phod1* and *shr-6* mutants were smaller than WT and accumulated visible levels of anthocyanin (Supplementary Fig. 5a,b). The roots of the mutants had longer and denser root hairs than the WT (Supplementary Fig. 5c). All these PSR phenotypes were rescued in *phod1* by complementation with native promoter-driven WT *SHR* (Supplementary Fig. 5a-c). In addition to *PHT1;4*, we examined the expression of other Pi starvation-induced (PSI) genes, and found that all genes were constitutively expressed in *phod1* or *shr-6* mutants (Supplementary Fig. 6a,b). Further analysis of the *phod1* transcriptome under Pi-replete condition revealed the upregulation of 282 PSI genes in the shoot, which accounted for

about 30% of all up-regulated genes in *phod1* (Fig. 1c,d). These results suggest that the *shr* mutant experiences Pi starvation even when grown under Pi-replete condition. We observed that the cellular Pi content was decreased dramatically in the shoots of *phod1* and *shr-6* mutants compared to WT and complementation lines, while Pi content increased in roots of the *shr* mutants (Fig. 1e). To elevate Pi absorption in the shoot of *phod1*, seedlings were submerged in Pi solution, which can gradually restore the expression levels of PSI genes in the shoot by improving Pi concentration in solution (Supplementary Fig. 6c).

SHR is expressed in the stele and the protein migrates to cortex to form a complex with SCR and activates *SCR* expression[3]. As expected, *SCR* transcription was dramatically repressed in *phod1* mutant (Supplementary Fig. 7a). Similar to *shr* mutants, the PSI genes were induced and the Pi content in shoot was decreased in *scr* mutant (Supplementary Fig. 7b,c).

To test the hypothesis that the constitutive PSR phenotypes of *phod1* resulted from either a defective shoot or root, we performed a reciprocal micrografting experiment with WT and *phod1* mutant seedlings. Although the *shr* mutation resulted in Pi deficiency symptoms, grafting rescued the mutant phenotype when *phod1* shoot was used as scion grafted onto the WT rootstock, similar to the WT scion control (Supplementary Fig. 8a,b). However, when *phod1* was used as rootstock, both *phod1* and WT scions accumulated higher levels of anthocyanin and were much smaller than those with WT-rootstock (Supplementary Fig. 8a,b). Consistent with the phenotype, Pi

concentration decreased dramatically in scions with *phod1* rootstock (Supplementary Fig. 8c). These evidences indicate that *phod1* root genotype is necessary and sufficient for decreased Pi concentration in the shoot. Our findings further suggest that SHR function in the root is required for Pi translocation from root to shoot.

The defect in translocating Pi from root to shoot in *phod1* is reminiscent of the *pho1* mutant[5,13]. *PHO1* transcript level was not significantly changed in the root of *shr* mutants (Fig. 2a). To determine the tissue-specific expression patterns of PHO1, we transformed *GFP*-fused *PHO1* driven by its native promoter (*PHO1-GFP*) into the *pho1* mutant. The resultant transgenic plants have the Pi content in the shoot restored, indicating that the fusion protein is functional (Supplementary Fig. 9). PHO1-GFP is expressed in the pericycle, predominantly in the xylem-pole pericycle cells. However, introduction of the *phod1* mutation into the *PHO1-GFP* transgenic line decreased the GFP signal dramatically (Fig. 2c). Consistent with the GFP signal, Western-blot analysis showed that the protein level of PHO1-GFP was much lower in *phod1* mutant than WT (Fig. 2b). To verify that Pi deficiency in the mutant is due to decreased PHO1 protein level, we attempted to increase its expression by transforming the *pPHO1::PHO1* construct into *phod1*. Although most transformants showed mutant phenotype, we identified two lines with high *PHO1* transcript levels in which the PSR phenotypes of *phod1* were partially rescued (Fig. 2d,e and Supplementary Fig. 10). The cellular Pi content in the overexpression lines was also significantly increased compared to the *phod1* mutant, although still lower than WT (Fig. 2e). PHO2-

149 dependent PHO1 degradation can be blocked by endosomal protease inhibitor E-64d[6].
150 We found that E-64d treatment significantly enhanced PHO1 protein in *phod1* (Fig. 2f),
151 and knocking out *PHO2* gene in *phod1* mutant significantly improved its Pi content,
152 although it was still lower than WT (Fig. 2g). These results indicated that *shr* mutation
153 repressed PHO1 post-transcriptionally.
154 As PHO2 regulates PHO1 degradation, we found enhanced *PHO2* transcript levels in
155 both *shr-6* and *scr-1* mutants (Fig. 3a). Analysis of the stele-specific microarray data[14]
156 also revealed higher expression levels of *PHO2* in *shr-2* mutant (Supplementary Fig.
157 11). SHR/SCR-activated microRNA miR165/166 can migrate from the endodermis to
158 the stele where they target the *PHB* mRNA and other transcripts of HD-ZIP III
159 transcription factors[15]. Therefore, the transcript levels of *PHB* increased in both *shr* and
160 *scr* mutants (Fig. 3a). Interestingly, mutation of *PHB* in *shr-2 phb-6* double mutant
161 repressed *PHO2* expression (Supplementary Fig. 11). Mutation of *PHB* also rescued
162 the PSR phenotypes, and partially restored cellular Pi content (Fig. 3b,c). As *PHB*
163 mRNA is targeted by miR165/166 for degradation, we fused the FLAG tag to a miRNA-
164 insensitive version of *PHB*[16], and transformed the native promoter-driven fusion gene
165 (*PHB*$_{en}$*-FLAG*) into WT to enhance *PHB* (*PHB*$_{en}$) expression. With the increase in *PHB*
166 expression, the *PHO2* transcript level was also increased in the transgenic lines
167 (Supplementary Fig. 12a,b). Therefore, it is likely that SHR regulates *PHO2* gene
168 expression through PHB. Since the *PHO2* promoter contains several putative PHB
169 binding sites (Supplementary Fig. 13), we tested whether PHB could bind to these
170 motifs. Both GST-fused full PHB and its HD-ZIP domain could bind to the P1 motif,

while the HD domain only or the C-terminal could not (Fig. 3d). Mutation of the critical amino acid residue (N76I) in the HD domain abolished the binding, which suggested that both HD and ZIP domains are necessary and sufficient for binding to the P1 region on the promoter (Fig. 3d). The binding of PHB to the P1 region was competitively blocked by an unlabeled P1 probe (Supplementary Fig. 14). Furthermore, the HD-ZIP domain could also bind to P2, P3, P4 and P5 motifs in the *PHO2* promoter with different affinities (Fig. 3e). The class III HD-ZIP family has five members (PHB, PHV, REV, CNA, ATHB8), all of which can be targeted by miR165/166; hence, their expressions were all increased in the *shr* mutant[15]. *In vitro* EMSA experiment showed that all five proteins could bind to the *PHO2* promoter (Supplementary Fig. 15). Both PHB_{en} and PHV_{en} could significantly activate *PHO2* expression in dual-LUC transient transcriptional assay (Fig. 3g). Furthermore, the chromatin immunoprecipitation (ChIP) assay using *PHB_{en}-FLAG* transgenic line showed that PHB_{en}-FLAG was enriched on the *PHO2* promoter *in vivo* (Fig. 3f). These data indicated that the SHR-mediated PHB directly regulates *PHO2* gene expression.

To assess SHR responsiveness to Pi starvation, we evaluated the relative abundance of *SHR* transcripts and the encoding protein in plants grown on medium containing different concentration of Pi (Fig. 4a and Supplementary Fig. 16). *SHR* transcription was induced in the roots under Pi starvation (Supplementary Fig. 16). However, SHR-FLAG protein levels decreased in root with decreasing availability of Pi (Fig. 4a,b), but not of nitrogen, to the plant (Supplementary Fig. 17). To avoid the side effect of root

193 growth inhibition mediated by photo-Fenton reaction[17], we covered the roots of *SHR-*
194 *FLAG* line with aluminum foil, and found that the SHR-FLAG protein still decreased
195 dramatically (Fig. 4c and Supplementary Fig. 18). We also confirmed this change
196 further in the *SHR-GFP* line (Fig. 4d and Supplementary movie 1a,b). The suppression
197 of SHR-FLAG by Pi deficiency could not be blocked by the addition of MG132, a 26S
198 proteasome inhibitor, or a mixed protease inhibitors cocktail (Fig. 4e). Besides, SHR-
199 FLAG protein immunoprecipitated from transgenic plants was incubated with total
200 proteins extracted from Col-0 plants grown on Pi-replete or Pi-depleted condition, and
201 the degradation rate of SHR-FLAG was similar (Fig. 4f). Furthermore, we examined
202 SHR protein stability by applying cycloheximide (CHX), a protein translation inhibitor,
203 to *SHR-FLAG* transgenic plants. Blocking of translation by CHX resulted in a similar
204 decline of SHR-FLAG protein under Pi-replete to Pi-depleted condition (Fig. 4g).
205 Therefore, these results suggest that Pi starvation represses SHR by inhibiting its
206 translation.
207 Consistent with the repression of SHR, PHB-GFP signal is stronger under Pi-depleted
208 condition than that under Pi-replete condition, especially at xylem pole (Fig. 4h and
209 Supplementary movie 2). As PHB activates PHO2, which directs PHO1 degradation,
210 PHO1-GFP abundance was rescued by *PHB* mutation in *phod1* mutant (Fig. 4i).
211 Although PHO1-GFP signal increased within 2 days on Pi-depleted medium, it
212 decreased after long-term Pi starvation (Fig. 4j). The change in PHO1-GFP was
213 confirmed by Western-blot (Fig. 4k), which was coincident with the decline of SHR
214 protein under long-term Pi starvation (Fig. 4l).

When seedlings are transferred to Pi deficiency condition, although Pi content decreases in both the shoot and the root, a higher proportion of Pi is allocated to the shoot during the early stage, but a reversal in the allocation strategy was observed under long-term Pi starvation. Accordingly, the Pi content root/shoot ratio was significantly increased under long-term Pi-depleted condition (Fig. 4m). Mutation of *SHR* in *phod1* mutant could mimic the Pi allocation strategy under Pi-deficient condition (Fig. 4n) and a similar result was also observed for total P content (Supplementary Fig. 19). These results indicate that Pi starvation represses SHR to regulate PHO1 abundance in xylem-pole pericycle cells to allocate a higher proportion of Pi to the root, which ensures root vitality to forage more Pi from the soil.

To respond to Pi deficiency, plants have evolved sophisticated strategies to orchestrate Pi uptake, usage and redistribution between shoot and root[18]. During the onset of Pi deficiency, miR399 was induced in the shoot and transduced as a systemic signal to the root where it targets *PHO2* mRNA, and thus PHO1 is stabilized[6]. Pi starvation also activates the ubiquitin E3 ligase PRU1 to direct the degradation of WRKY6, releasing its repression on *PHO1* gene expression[7,8]. Enhanced PHO1 level aids the allocation of more Pi to the shoot to stimulate photosynthesis. However, after long-term Pi deficiency, SHR is repressed to reduce PHO1 to limit Pi translocation from root to shoot, and more Pi is retained in the root to support its vitality and expansion to forage more Pi from the soil (Fig. 4o). To support this, the root:shoot ratio increases in terms of both biomass and Pi content (Fig. 4m,n and Supplementary Fig. 1). Here, we provide biochemical and molecular evidences that Pi starvation represses SHR to release the downstream

transcription factor PHB, which directly regulates *PHO2* transcription to promote PHO1 degradation inhibiting Pi translocation from roots to shoots.

Methods

Plant materials and growth conditions

The following transgenic lines have been described previously: *pSCR::GFP*[19], *pPHT1;4::LUC* and *pPHT1;4::GUS*[11,20]. For the following *Arabidopsis* mutants, seeds were ordered from *Arabidopsis* Biological Resource Center (ABRC): *shr-6* (SALK_002744), *pho1-2* (CS8507), *pho2* (SAIL_47_E01), *phb* (SALK_008924, SALK_021684). *shr-6 phb* double mutant was generated by genetic cross between *shr-6* and *phb*. Plants were grown in half-strength Murashige and Skoog (1/2 MS) agar medium with 1.0% (w/v) sucrose, and 1.1% (w/v) agar under 16 h/8 h light/dark cycle at 23 °C.

Mutant isolation and mapping-by-sequencing analysis

EMS-mutagenized M_2 seeds were sowed directly on 1/2 MS medium plates. 100 mM luciferin was sprayed on the 8-day-old seedlings and the fluorescence images were taken with a CCD camera (PyLoN1300B, Princeton Instruments). Seedlings with enhanced LUC signal were selected as candidates, and the phenotype was confirmed in the next generation. To map the mutated genes, mutants were back-crossed to WT and a total of 250 F_2 seedlings with enhanced LUC signal were pooled and the genomic DNA was isolated to perform next generation sequencing. The sequencing reads were mapped to the *Arabidopsis* genome (version TAIR10) with SHORE and GenomeMapper[12,21], and candidate causative mutations were identified with algorithms developed in SHOREmap v.3.0.

Plasmid construction and complementation analysis

For complementation, *SHR* genomic DNA with about 2 kb promoter region was amplified from Col-0 genomic DNA and cloned into pCAMBIA1300 vector harboring a C-terminal GFP or FLAG tag by homologous recombination method. Mutation site was introduced into *SHR* through site-directed mutagenesis with primers listed in supplementary Table S1. *PHO1* genomic DNA with about 2 kb native promoter region was cloned into pCAMBIA1300 vector harboring C-terminal GFP tag. *PHB* genomic DNA with about 2 kb promoter was cloned into pCAMBIA1300 and mutation in miR165/166 target site was introduced into *PHB* using primers listed in supplemental Table S1. The construct was transformed into WT plants. *Agrobacterium* strain GV3101 was used to transform the constructs into different genotypes by the standard floral dip method[22].

Pi, total P and anthocyanin estimation

To determine Pi content, the tissues of 8-day-old seedlings were collected in 1.5 ml Eppendorf tubes and ground into fine powder by metal beads after snap-freezing in liquid nitrogen. Pi content was then measured using the phosphomolybdate colorimetric assay as described[23]. Elemental analysis of total P through ICP-MS was performed as previously described[24]. Shoot and root of 12-day-old seedlings on P+ or P- conditions were separately collected, and subsequently rinsed with deionized water four times. After drying at 65°C for three days and cooling in room temperature, each sample was

weighed in triplicate or in quadruplicate on an analytical balance. All samples were digested by concentrated nitric acid and further estimation of total P was performed on a NexION 350d ICP-MS spectrometer (PerkinElmer) coupled with an Apex desolvation system and an SC-4 DX autosampler (Elemental Scientific). As previously described, all the samples were normalized with a heuristic algorithm[25]. For anthocyanin estimation, anthocyanin was extracted with methanol containing 1% HCl (v/v). After removal of chlorophyll with an equal volume of chloroform, the anthocyanin content was measured as described[26]. Relative anthocyanin contents were calculated and shown as $A_{530-657}$ g^{-1} fresh weight.

Grafting of *Arabidopsis* plants

Five-day-old seedlings grown on 1/2 MS medium were used to do the reciprocal grafting under dissecting microscope in clean hood as described(Bainbridge et al., 2014). Two-week-old grafted plants without adventitious roots were used for the subsequent analyses.

Histochemical analysis and microscopy

Histochemical GUS staining was assayed as previously described[20]. The GUS-stained seedlings were photographed using a microscope (Zeiss Imager M2).

Real-Time quantitative PCR

Total RNA was extracted from shoot or root using the RNeasy Plant Kit (Qiagen), and

1 μg RNA was reverse-transcribed following the manufacturer's instructions (YESEN, 11121ES60). The cDNA was used as template and real-time PCR was performed on a CFX96 real-time PCR detection system (Bio-RAD). *ACT2* was used as the reference gene. The primers used in RT-qPCR are listed in Table S1.

Transcriptome analysis

The shoot of 8-day-old wild-type and *phod1* under P+ conditions were collected in triplicate. Total RNA was extracted via the RNeasy Plant Kit (Qiagen) and adding DNase to digest genomic DNA contamination during isolation of RNA. RNA-Seq was carried out with the Illumina HiSeq 2000 platform and the clean reads were mapped to *Arabidopsis* genome build TAIR10 using the aligner STAR version 2.5.3a[27]. The quantification was carried out with StringTie version 1.3.3[28]. Differentially expressed genes were analyzed using DESeq2, an R/Bioconductor package[29]. The genes that were either up- or downregulated with a two-fold or higher change with an adjusted P value of ≤ 0.05 were regarded as differentially expressed genes (DEGs). GO enrichment analysis of the DEGs was performed using clusterProfiler[30]. The list of the DEGs is available in Supplemental Dataset 1.

Western blotting

To determine the SHR-GFP, SHR^{phod1}-GFP, SHR-FLAG or PHO1-GFP protein levels, seedling tissues were ground into fine powder in liquid nitrogen and dissolved in 5% SDS. Then the solution was boiled in 95°C for 5 min and centrifuged for 10 min at

13,000 rpm. The supernatant was mixed with 5×SDS loading buffer and separated on a 10% SDS-PAGE gel. Anti-GFP (Roch), anti-FLAG (Sigma) and anti-ACTIN (CWBIO) antibodies were used to detect the proteins.

Transient expression assays in *Arabidopsis* protoplasts

Briefly, 5-d-old *Arabidopsis* seedlings were harvested from 1/2 MS solid medium. Roots were shredded in 10 ml enzyme digestion solution (1.5% cellulose, 1.5% pectolyase, 0.4 M mannitol, 20 mM MES, 20 mM KCl, 10 mM $CaCl_2$, 0.1% BSA). The digestion solution was gently shaken at 80 rpm for 2 h. Protoplasts were harvested for plasmid transformation including effectors, reporter and internal control. The plasmid transformation in protoplasts, LUC and GUS activity assays was performed as described[31].

Protein degradation assays *in vitro*

SHR-FLAG protein of 8-day-old seedlings was immunoprecipitated and purified using beads fused with FLAG antibody, and the SHR-FLAG protein was equally divided into PCR tubes. Total protein of wild-type seedlings under P+ or P- conditions was crudely extracted by solution (20 mM Tris-HCl, 150 mM NaCl, pH=7.4). After protein quantification, equal amount of crude proteins from P+ and P- conditions was added into the PCR tube for the degradation of SHR-FLAG for 5, 15, 30 and 60 min in room temperature. 5% SDS was added to the tube and immediately boiled in 95 °C for 5 min to terminate the degradation reaction. The SHR-FLAG level was assayed by Western-

blot, while ACTIN protein acting as the indicator for equivalent crude proteins from P+ or P- in reaction.

Chromatin Immunoprecipitation (ChIP) assays

Roots of seedlings were collected and immediately cross-linked in 1% formaldehyde as previously described[32]. Protein A/G Magnetic Beads (MCE, HY-K0202) were used for pre-clearing samples and antibody binding. Anti-FLAG (Sigma, F1804) was used for immunoprecipitation of protein with FLAG. ChIP products were eluted with 50 μL of ddH_2O, and 1 μL product was used as template for each qPCR reaction. The primers for ChIP-qPCR are listed in Table S1.

Electrophoretic mobility shift assay (EMSA)

Expression and purification of GST-fused proteins in *E. coli* BL21 were performed as previously described[33]. The binding sites of HD-ZIP III protein on *PHO2* promoter was analyzed using an online resource AthaMap[34]. Biotin-labeled probes (30 bp DNA) and non-biotin-labeled competitor probes were chemically synthesized (Sangon Biotech, Shanghai, China). 1 μg of recombinant protein and 50 fmol probe or additional dose of competitors was mixed in a reaction volume of 20 μL for DNA-protein binding assay. EMSA was performed using a Pierce™ LightShift® Chemiluminescent EMSA Kit (Thermo Scientific, USA) according to the manufacturer's instructions. Migration of biotin-labeled probes was detected using ECL and ChemDoc imaging system (Bio-Rad, USA). All of the probe or competitor sequences used in EMSA are listed in Table S1.

Accession Numbers

Gene sequences reported in this article can be found in the *Arabidopsis* Genome Initiative and the locus numbers are as follows: *SHR* (AT4G37650), *SCR* (AT3G54220), *MIR165a* (AT1G01183), *MIR166b* (AT4G00885), *PHB* (AT2G34710), *PHV* (AT1G30490), *REV* (AT5G60690), *CNA* (AT1G52150), *ATHB8* (AT4G32880), *PHO1* (AT3G23430), *PHO2* (AT2G33770). *PHT1;1* (At5G43350), *PHT1;4* (At2G38940), *PHT1;5* (AT2G32830), *IPS1* (At3G09922), *AT4* (AT5G03545), *SPX1* (AT5G20150), *RNS1* (AT2G02990), *PAP17* (AT3G17790), *MIR399c* (AT5G62162), *MGD3* (AT2G11810), *PAP10* (AT2G16430).

Acknowledgments

This work was supported by the Shanghai Sailing Program (20YF1456100) and Chinese Academy of Sciences (CAS).

Figure legends

Fig. 1. SHR is required for Pi translocation to shoot. a, Comparison of *LUC* expression driven by *pPHT1;4* promoter (top part) on 1/2 MS medium among WT, *phod1* mutant, and *phod1* transformed with GFP-fused *SHR* driven by its native promoter. Scale bars 0.5 cm. **b**, Expression level of endogenous *PHT1;4* gene in WT, *phod1* mutant and *phod1* transformed with GFP-fused *SHR* driven by its native promoter. Error bars are mean ± s.d. Sets of data were analyzed by independent-samples T test (two-tailed), where two asterisks and one asterisk represent statistically significant difference at $p < 0.01$ and $p < 0.05$, respectively. **c**, Cluster display of transcripts of Pi starvation-induced (PSI) genes up-regulated in the shoot of *phod1* mutant. **d**, Diagram showing the number of genes up-regulated by Pi starvation and *phod1* mutation. **e**, Pi content in shoot or root of different genotypes shown in (**a**). Error bars are mean ± s.d. with four biological replicates and measured twice. Sets of data were analyzed by one-way ANOVA followed by Tukey post hoc test, where letters represent statistically significant difference at $p < 0.05$ for multiple comparisons.

Figure 2. PHO1 localization pattern and protein levels are altered in *phod1*. a, Quantitative analysis of *PHO1* gene expression in the shoot and root of WT, *shr-6*, *phod1*, *SHR-GFP/pho1*. Error bars are mean ± s.d. Sets of data were analyzed by independent-samples T test (two-tailed). **b**, Western-blot analysis of PHO1-GFP protein level in the root of WT or *phod1*. NC: negative control. **c**, PHO1-GFP fusion protein fluorescence in WT or *phod1*. Green signal represents GFP fluorescence; red signal

represents propidium iodide (PI) staining. The white arrow heads mark the endodermal transversal wall (the position of Casparian strip) at which PI is blocked. Ep: epidermis; Co: cortex; En: endodermis; Xy: xylem. Scale bars 20 μm. **d-e**, Morphological appearance (**d**) and Pi content (**e**) of 2-week-old WT, *phod1*, and transgenic lines with different expression level of *PHO1*. Scale bars 0.5 cm (**d**). Error bars are mean ± s.d. with three biological replicates. Sets of data were analyzed by one-way ANOVA followed by Tukey post hoc test, where letters represent statistically significant difference at $p < 0.05$ for multiple comparisons (**e**). **f**, Western blot analysis of PHO1 in root of WT or *phod1* after E64d treatment. 4-day-old seedlings were treated with E64d for three consecutive days. Roots were collected for total protein extraction and Western-blot analysis. **g**, Pi content in the shoot of 9-day-old seedlings of WT, *phod1* and *phod1 pho2* double mutant. Error bars are mean ± s.d. with three biological replicates and measured twice. Sets of data were analyzed by one-way ANOVA followed by Tukey post hoc test, where letters represent statistically significant difference at $p < 0.05$ for multiple comparisons.

Figure 3. PHB directly regulates *PHO2* expression. a, Quantitative analysis of *PHB* and *PHO2* gene expression in the root of Col-0, *shr-6* and *scr-1* on Pi-sufficient conditions. Error bars are mean ± s.d. The bar graph shows results from three biological replicates. Sets of data were compared by independent-samples T test (two-tailed), where three asterisks and two asterisks represent statistically significant difference at $p < 0.001$ and $p < 0.01$, respectively, compared to WT. **b**, Anthocyanin phenotype in the leaves of Col-0, *phb*, *shr-6*, and the *shr-6 phb* double mutant. **c**, Pi content in the shoot

or the root of different genotypes in (**b**). The bar graph shows results from 2-3 biological replicates and measured twice. Sets of data were compared by independent-samples T test (two-tailed), where three asterisks represent statistically significant difference at $p < 0.001$. **d**, Electrophoretic mobility shift assay (EMSA) of full-length and truncated PHB protein binding to P1 motif of *PHO2* promoter. Bio: biotin; FL: full-length. **e**, EMSA of HD-ZIP domain of PHB binding to different motifs in *PHO2* promoter. N1 and N2 probes acted as negative controls. **f**, Enrichment of PHB protein on *PHO2* promoter in positions shown in red in the schematic diagram. Col-0 acts as a control. TSS: transcription start site. Error bars are mean ± s.d. Sets of data were analyzed by independent-samples T test (two-tailed), where three asterisks and two asterisks represent statistically significant difference at $p < 0.001$ and $p < 0.01$ compared to control. **g**, Transient expression of enhanced PHB or PHV activates the transcription driven by *PHO2* promoter in root protoplast. *pUBQ-GUS* acts as an internal control. Error bars are mean ± s.d. with three biological replicates. The three asterisks and one asterisk represent statistically significant difference at $p < 0.001$ and $p < 0.05$, respectively, compared to control analyzed by independent-samples T test (two-tailed).

Figure 4. Decrease in SHR level in root restricts Pi allocation to shoot under long-term Pi starvation. a, Protein level of SHR in root of transgenic line under different Pi concentrations. ACTIN protein acts as the loading control. **b**, SHR protein level in root differentiation zone under Pi-sufficient (P+) or Pi-deficient (P-) conditions. **c**, SHR protein level in root under shading under P+ or P- conditions. **d**, GFP-fused SHR fluorescence indicates the localization and protein level of SHR in root differentiation

458 zone under P+ or P- conditions with root shading. Scale bars 40 μm. **e**, SHR protein
459 level on adding protease inhibitors, K^+ or Pi under P- conditions for 2 days. The
460 components of Cocktail include protease inhibitors AEBSF, Aprotinin, Bestatin, E-64,
461 Leupeptin and Pepstatin A. Pi was added in the form of 1.25 mM KH_2PO_4. **f**,
462 Degradation of SHR protein *in vitro* by incubating equivalent amounts of total protein
463 obtained from P+ or P- seedlings sampled at various timepoints. **g**, SHR protein level
464 when seedlings are moved from P+ to P+ or P+ to P- conditions by adding protein
465 translation inhibitor CHX for three consecutive days. **h**, GFP-fused PHB fluorescence
466 indicates PHB protein level under P+ or P- conditions. Scale bar 20 μm. **i**, PHO1-GFP
467 green fluorescence in root differentiation zone of *phod1* or *phod1 phb* double mutant
468 (*PHB* knock-out). Scale bar 20 μm. **j**, GFP-fused PHO1 protein abundance indicated
469 by green fluorescence in root differentiation zone under short-term (2 days) or long-
470 term (7 days) Pi deficiency conditions. Scale bar 20 μm. **k**, Western-blot analysis of
471 PHO1 protein level in root treated with short-term (2 days) or long-term (7 days) Pi
472 deficiency condition. **l**, Protein level of SHR in root of 9-days seedlings suffer from
473 short-term or long-term Pi deficiency. **m**, Pi content and its root/shoot ratio for WT
474 plants treated by short-term or long-term Pi deficiency. Error bars are mean ± s.d. with
475 three or four biological replicates and measurements were repeated twice. Sets of data
476 were analyzed by one-way ANOVA followed by Tukey post hoc test where letters
477 represent statistically significant difference at $p < 0.05$ for multiple comparisons. **n**,
478 Decrease in SHR level elevates the root/shoot Pi content ratio in WT plants under P-
479 condition, or in *phod1* on P+ condition for long-term (9 days). Error bars are mean ±

s.d. with three biological replicates and measured thrice. Sets of data were analyzed by one-way ANOVA followed by Tukey post hoc test where letters represent statistically significant difference at $p < 0.05$ for multiple comparisons. **o**, A model for SHR regulating Pi translocation between root and shoot. Under Pi-sufficient condition, SHR is required to maintain PHO1 expression in root xylem-pole pericycle and support Pi translocation to shoot. During the early stages of Pi deficiency, PHO1 protein is enhanced in root by transcriptional and post-transcriptional regulators. However, long-term or serious Pi deficiency post-transcriptionally inhibits SHR and PHB increases in the root stele. PHO1 is suppressed by PHO2 and/or other factors. Therefore, a limited amount of Pi is locked in the root which is essential for root vitality and root expansion to forage more Pi under scarcity or in soils with heterogeneous distribution of Pi.

Supplementary Fig. 1. Pi availability regulates biomass and Pi allocation proportion between shoot and root. a, Phenotype of *Arabidopsis* seedlings grown on different Pi concentrations for 8 days. Scale bar 0.5 cm. **b**, Biomass and root/shoot ratio for seedlings grown on different Pi concentrations. **c**, Pi content and Pi root/shoot ratio for seedlings grown on various phosphate conditions. Error bars are mean ± s.d with three biological replicates. Sets of data were compared by one-way ANOVA followed by Tukey post hoc test, where letters represent statistically significant difference at $p < 0.05$ for multiple comparisons.

Supplementary Fig. 2. Identification of the causal mutation in *phod1* mutant through mapping-by-sequencing. a, The *phod1* mutant was screened by enhanced

luminance signal. **b**, F_2 progeny segregated 3:1 (WT: mutant) ratio suggesting a single recessive mutation. The *phod1* mutant was crossed with WT to get the BC_1F_1 plant, which was then selfed to get the BC_1F_1 population. The BC_1F_2 population was deep sequenced. **c**, Visualization of allele frequency estimations in the backcross population. The average allele frequencies (200 kb windows and 50 kb step size) are shown as the blue line. The mapping interval predicted on chromosome 4 is demarcated with a red arrow. **d**, Schematic diagram showing the mutation sites in *phod1* and Sanger sequencing chromatogram showing one base mutation (C866T) in *phod1*. **e**, Comparison of *pPHT1;4::GUS* expression among WT and *phod1* mutant. Scale bars 0.5 cm.

Supplementary Fig. 3. Functional complementation of *phod1* mutant with FLAG-fused SHR. a, Phenotype of *phod1* complementation lines. The *phod1* mutant was transformed with *SHR-FLAG* driven by its native promoter on Pi-sufficient (P+) conditions. Scale bar 0.5 cm. **b**, Pi content in shoot of WT, *phod1* and transgenic lines of SHR-FLAG to *phod1*shown in (**a**). Error bars are mean ± s.d. with three biological replicates and the measurements were repeated twice thrice. Sets of data were analyzed by one-way ANOVA and Tukey's post hoc tests where letters represent statistically significant difference at $p < 0.05$ for multiple comparisons.

Supplementary Fig. 4. *phod1* is a weak allele of *SHR*. a, Comparison of the root growth among WT, *phod1* and *shr-6* mutants, *shr-6* transformed with GFP-fused mutated or wild-type SHR driven by its native promoter. Scale bar 0.5 cm. **b**,

Comparison of root apical meristem of WT, *phod1* and *shr-6* seedlings grown on 1/2 MS medium for 8 days. Ep: epidermis; Gt: ground tissue, including cortex and endodermis; St: stele. White asterisks indicate QC cells. Scale bar 20 μm. **c**, Analysis of endogenous *SHR* gene expression by real-time qPCR in WT, *phod1* and *shr-6*. Error bars are mean ± s.d. with three biological replicates. Sets of data were analyzed by independent-samples T test (two-tailed), where three and two asterisks represent significant difference at $p < 0.001$ and $p < 0.01$, respectively, compared to WT. **d** and **e,** Analyses of *SHR-GFP* transcript (**d**) and protein (**e**) levels in SHR^{WT}*-GFP* or SHR^{phod1}*-GFP* transgenic lines. **f**, GFP fluorescence analysis of SHR^{WT}-GFP and SHR^{phod1}-GFP protein in the root tips. Scale bar 25 μm. **g**, Inhibition of SHR^{phod1}-GFP degradation by treatment with MG132, the 26S proteasome inhibitor. NC: non-transgenic line as negative control. **h-j**, Shoot phenotypes **(h)** of WT, *phod1, shr-6,* transgene lines SHR^{phod1}*-GFP/shr-6* and *SHR-GFP/shr-6,* including anthocyanin content **(i)** and Pi content **(j)**. Error bars are mean ± s.d. with 2-3 biological replicates for (**i**), and 2-3 biological replicates and twice repeat-measurements for (**j**). Sets of data were analyzed by one-way ANOVA followed by Tukey post hoc test, where letters represent statistically significant difference at $p < 0.05$ for multiple comparisons.

Supplementary Fig. 5. Misregulation of PSR in *shr* mutants. a, Shoot morphological appearance of 9-day-old WT, *shr-6* and *phod1* mutants, and *phod1* mutant transformed with GFP-fused SHR driven by its native promoter. Scale bar 0.5 cm. **b**, Anthocyanin content in the shoot of different genotypes shown in (**a**). Error bars are mean ± s.d. with

three or six biological replicates. Sets of data were analyzed by one-way ANOVA followed by the Tukey post hoc test, where letters represent statistically significant difference at $p < 0.05$ for multiple comparisons. **c**, Microscopic images of root middle parts and root tips with intact root hair from 4-day-old seedlings of different genotypes. Scale bar 1.0 mm.

Supplementary Fig. 6. Misregulation of Pi starvation-induced (PSI) genes in *shr* mutants. a, Quantitative analysis of *IPS1* and *PHT1;1* gene expression in shoot or root of different genotypes under P+ condition. **b,** Verification of a group of up-regulated PSI genes in shoot of *phod1* by qPCR. c, Submersion of seedlings in ascending Pi medium to restore PSI genes expression in shoot of *phod1*. The asterisk represents significant difference at $p < 0.05$ compared with WT.

Supplementary Fig. 7. *scr* mutant exhibits Pi deficiency in shoot. a, *SCR* expression in the endodermis was dramatically reduced in *phod1* as observed through microscopy of pSCR::GFP green fluorescence. **b,** PSI genes (*IPS1* and *PHT1;4*) were induced in shoot of *scr* under P+ condition. Error bars are mean ± s.d. with three biological replicates. Sets of data were analyzed by independent-samples T test (two-tailed), and three asterisks represent significant difference at $p < 0.001$. **c,** Pi content was significantly reduced in the shoot of *scr* mutant. Error bars are mean ± s.d. with three biological replicates and measurements were repeated twice. Sets of data were analyzed by one-way ANOVA followed by Tukey post hoc test where the letters represent statistically significant difference at $p < 0.05$ for multiple comparisons.

Supplementary Fig. 8. Reciprocal grafting shows that Pi deficiency in the *phod1* shoot is driven by the root. a, Shoot morphological appearance of the grafted plants. Scale bar 0.5 cm. **b**, Anthocyanin accumulation in the leaves of the grafted plants. Scale bars, 0.1 cm. **c**, Pi content in shoot of the grafted plants. Error bars are mean ± s.d. with three biological replicates and measurements were repeated thrice. Sets of data were analyzed by one-way ANOVA followed by Tukey post hoc test and the letters represent statistically significant difference at $p < 0.05$ for multiple comparisons.

Supplementary Fig. 9. Transformation of *phod1* mutant with *pPHO1::PHO1-GFP*. Error bars are mean ± s.d. with three biological replicates. Sets of data were analyzed by independent-samples T test (two-tailed), and three or one asterisk represents significant difference at $p < 0.001$ or $p < 0.05$, respectively, compared with Col-0.

Supplementary Fig. 10. Detection of *PHO1* expression levels in *pPHO1::PHO1* transformed *phod1* mutant. Error bars are mean ± s.d. Sets of data were compared to *phod1* one-way ANOVA followed by Tukey post hoc test, where an asterisk represents a statistically significant difference at $p < 0.05$ for multiple comparisons.

Supplementary Fig. 11. Increase in PHB level activates *PHO2* expression in root stele cells. The transcript levels of HD-ZIP III family *PHB*, *PHV*, *REV*, *CNA* and *ATHB8* were increased in *shr-2* mutant. *IPT7* is a positive control reported to be directly activated by PHB. *SCR* and *SCL3* also act as controls activated by SHR. *PHO1*, *PHR1* and *PHL1* are negative controls whose transcript levels are not regulated by SHR or

PHB. The raw microarray expression profiles were collected from published data (Sebastian et al., 2015) and presented as a heatmap.

Supplementary Fig. 12. Up-regulation of PHB facilitates *PHO2* gene expression. a, Modification of basic group in *PHB* or *PHV* at the *miR165a* target site for transcript accumulation but without amino acid changes. **b,** Transcript level of *PHO2* in PHB up-regulated transgenic lines. Error bars are mean ± s.d. Sets of data were compared to Col-0 one-way ANOVA followed by Tukey post hoc test where an asterisk represents a statistically significant difference at $p < 0.05$ for multiple comparisons.

Supplementary Fig. 13. The HD-ZIP III binding sites in *PHO2* promoter as predicted by AthaMap. a, The list of candidate TFs and binding positions in *PHO2* promoter. The item was ranked by the score. **b,** Conserved binding sequence of the HD-ZIP III protein ICU4/CNA. **c,** Visualization of HD-ZIP proteins binding site on *PHO2* promoter according to the list in **(a)**.

Supplementary Fig. 14. **Competition test confirms PHB protein binding to P1 motif of *PHO2* promoter.** The binding of PHB to *PHO2* region was competitively blocked by unlabeled P1 probe. Com: competitor probe.

Supplementary Fig. 15. The HD-ZIP III proteins redundantly bind *PHO2* promoter. a, Phylogenetic tree of HD-ZIP III proteins based on the alignment of protein sequences. **b,** Percent identity of HD-ZIP domain of HD-ZIP III family proteins. **c,** Protein sequence alignment of HD-ZIP domain among PHB, PHV, REV, CNA and

ATHB8. **d,** HD-ZIP domain of PHB, PHV, REV, CNA and ATHB8 can bind the P1 site of *PHO2* promoter by EMAS test.

Supplementary Fig. 16. *SHR* transcript levels in root of WT under various phosphate conditions. Error bars are mean ± s.d. with three biological replicates. Sets of data were analyzed by one-way ANOVA followed by Tukey post hoc test where letters represent statistically significant difference at $p < 0.05$ for multiple comparisons.

Supplementary Fig. 17. SHR protein level is not altered under nitrogen deficiency conditions. a, Phenotype of *Arabidopsis* seedlings under nitrogen deficiency conditions. Nitrate was used as the nitrogen source. Scale bar 0.5 cm. **b,** Analysis of SHR protein level by Western-blot in root of seedlings under different nitrogen conditions. ACTIN was used as an internal protein control.

Supplementary Fig. 18. Root shading restores Arabidopsis primary root elongation under Pi-depleted condition. a, Experimental set up for root shading by aluminium-foil. **b**, Root morphology for lighting or shading under P+ or P- conditions. Scale bar 0.5 cm.

Supplementary Fig. 19. The total P root:shoot ratio increases in *phod1* mutant under P+ condition. Total P content and total P ratio of root/shoot for WT grown on P+ or P- conditions, or *phod1* grown on P+ condition long term (12 days). Error bars are mean ± s.d. with three or four biological replicates. Sets of data were analyzed by independent-samples T test (two-tailed), where three asterisks represent statistically

significant difference at $p < 0.001$ compared to WT. P+ (625 μM Pi); P- (30 μM Pi).

Supplementary Data Set 1. List of differentially expressed genes (DEGs) in wild-type versus *phod1* mutant.

Supplementary Table 1. Sequences of primers used in this study.

Supplementary movie 1. GFP-fused SHR protein abundance indicated by green fluorescence in root differentiation zone driven by its native promoter under Pi-sufficient (**a**) or Pi-deficient (**b**) conditions.

Supplementary movie 2. GFP-fused PHB protein abundance indicated by green fluorescence in root differentiation zone driven by its native promoter under Pi-sufficient (**a**) or Pi-deficient (**b**) conditions.

References

1 Benfey, P. N. *et al.* Root development in *Arabidopsis*: four mutants with dramatically altered root morphogenesis. *Development* **119**, 57-70 (1993).

2 Helariutta, Y. *et al.* The SHORT-ROOT gene controls radial patterning of the Arabidopsis root through radial signaling. *Cell* **101**, 555-567 (2000).

3 Cui, H. *et al.* An evolutionarily conserved mechanism delimiting SHR movement defines a single layer of endodermis in plants. *Science* **316**, 421-425 (2007).

4 Rouached, H. *et al.* Regulation of phosphate starvation responses in plants: signaling players and cross-talks. *Mol. Plant* **3**, 288-299 (2010).

5 Hamburger, D. *et al.* Identification and characterization of the Arabidopsis *PHO1* gene involved in phosphate loading to the xylem. *Plant Cell* **14**, 889-902 (2002).

6 Liu, T.-Y. *et al.* PHO2-dependent degradation of PHO1 modulates phosphate homeostasis in *Arabidopsis*. *Plant Cell* **24**, 2168-2183 (2012).

7 Chen, Y.-F. *et al.* The WRKY6 transcription factor modulates *PHOSPHATE1* expression in response to low Pi stress in *Arabidopsis*. *Plant Cell* **21**, 3554-3566 (2009).

8 Ye, Q. *et al.* The ubiquitin E3 ligase PRU1 regulates WRKY6 degradation to modulate phosphate homeostasis in response to low-Pi stress in Arabidopsis. *Plant Cell* **30**, 1062-1076 (2018).
9 Silva-Navas, A. *et al.* Role of cis-zeatin in root responses to phosphate starvation. *New Phytol.* **224**, 242-257, doi:10.1111/nph.16020 (2019).
10 Hermans, C. *et al.* How do plants respond to nutrient shortage by biomass allocation? *Trends Plant Sci.* **11**, 610-617, doi:10.1016/j.tplants.2006.10.007 (2006).
11 Lei, M. *et al.* Genetic and genomic evidence that sucrose is a global regulator of plant responses to phosphate starvation in Arabidopsis. *Plant Physiol.* **156**, 1116-1130 (2011).
12 Schneeberger, K. *et al.* SHOREmap: simultaneous mapping and mutation identification by deep sequencing. *Nat. Methods* **6**, 550-551 (2009).
13 Arpat, A. B. *et al.* Functional expression of PHO1 to the Golgi and trans-Golgi network and its role in export of inorganic phosphate. *Plant J.* **71**, 479-491 (2012).
14 Sebastian, J. *et al.* PHABULOSA controls the quiescent center-independent root meristem activities in *Arabidopsis thaliana*. *PLoS Genet.* **11**, e1004973, doi:10.1371/journal.pgen.1004973 (2015).
15 Carlsbecker, A. *et al.* Cell signalling by microRNA165/6 directs gene dose-dependent root cell fate. *Nature* **465**, 316-321 (2010).
16 Miyashima, S. *et al.* Non-cell-autonomous microRNA165 acts in a dose-dependent manner to regulate multiple differentiation status in the *Arabidopsis* root. *Development* **138**, 2303-2313, doi:10.1242/dev.060491 (2011).
17 Zheng, Z. *et al.* Blue light-triggered chemical reactions underlie phosphate deficiency-induced inhibition of root elongation of *Arabidopsis* seedlings grown in petri dishes. *Mol. Plant* **12**, 1515-1523 (2019).
18 Chiou, T. J. & Lin, S. I. in *Annu. Rev. Plant Biol.* Vol. 62 *Annual Review of Plant Biology* 185-206 (2011).
19 Laurenzio, L. D. *et al.* The SCARECROW Gene Regulates an Asymmetric Cell Division That Is Essential for Generating the Radial Organization of the Arabidopsis Root. *Cell* **86**, 423-433 (1996).
20 Lei, M. *et al.* Ethylene signalling is involved in regulation of phosphate starvation-induced gene expression and production of acid phosphatases and anthocyanin in *Arabidopsis*. *New Phytol.* **189**, 1084-1095 (2011).
21 Schneeberger, K. *et al.* Simultaneous alignment of short reads against multiple genomes. *Genome Biol.* **10**, R98, doi:10.1186/gb-2009-10-9-r98 (2009).
22 Clough, S. J. & Bent, A. F. Floral dip: A simplified method for *Agrobacterium*-mediated transformation of *Arabidopsis thaliana*. *Plant J.* **16**, 735-743 (1998).
23 Jain, A. *et al.* Differential effects of sucrose and auxin on localized phosphate deficiency-induced modulation of different traits of root system architecture in Arabidopsis. *Plant Physiol.* **144**, 232-247 (2007).
24 Danku, J. M. C. *et al.* Large-scale plant ionomics. *Methods in molecular biology (Clifton, N.J.)* **953**, 255-276 (2013).

25 Lahner, B. *et al.* Genomic scale profiling of nutrient and trace elements in Arabidopsis thaliana. *Nat. Biotechnol.* **21**, 1215-1221 (2003).
26 Bieza, K. & Lois, R. An Arabidopsis mutant tolerant to lethal ultraviolet-B levels shows constitutively elevated accumulation of flavonoids and other phenolics. *Plant Physiol.* **126**, 1105-1115 (2001).
27 Dobin, A. *et al.* STAR: ultrafast universal RNA-seq aligner. *Bioinformatics* **29**, 15-21 (2013).
28 Pertea, M. *et al.* StringTie enables improved reconstruction of a transcriptome from RNA-seq reads. *Nat. Biotechnol.* **33**, 290-295 (2015).
29 Love, M. I. *et al.* Moderated estimation of fold change and dispersion for RNA-seq data with DESeq2. *Genome Biol.* **15**, 550, doi:10.1186/s13059-014-0550-8 (2014).
30 Yu, G. *et al.* clusterProfiler: an R Package for Comparing Biological Themes Among Gene Clusters. *Omics-a Journal of Integrative Biology* **16**, 284-287, doi:10.1089/omi.2011.0118 (2012).
31 Yoo, S.-D. *et al.* Arabidopsis mesophyll protoplasts: a versatile cell system for transient gene expression analysis. *Nat. Protoc.* **2**, 1565-1572 (2007).
32 Saleh, A. *et al.* An efficient chromatin immunoprecipitation (ChIP) protocol for studying histone modifications in Arabidopsis plants. *Nat. Protoc.* **3**, 1018-1025 (2008).
33 Xiao, X. *et al.* A group of SUVH methyl-DNA binding proteins regulate expression of the DNA demethylase ROS1 in *Arabidopsis*. *J. Integr. Plant Biol.* **61**, 110-119 (2019).
34 Steffens, N. O. *et al.* AthaMap: an online resource for *in silico* transcription factor binding sites in the *Arabidopsis thaliana* genome. *Nucleic Acids Res.* **32**, D368-D372 (2004).

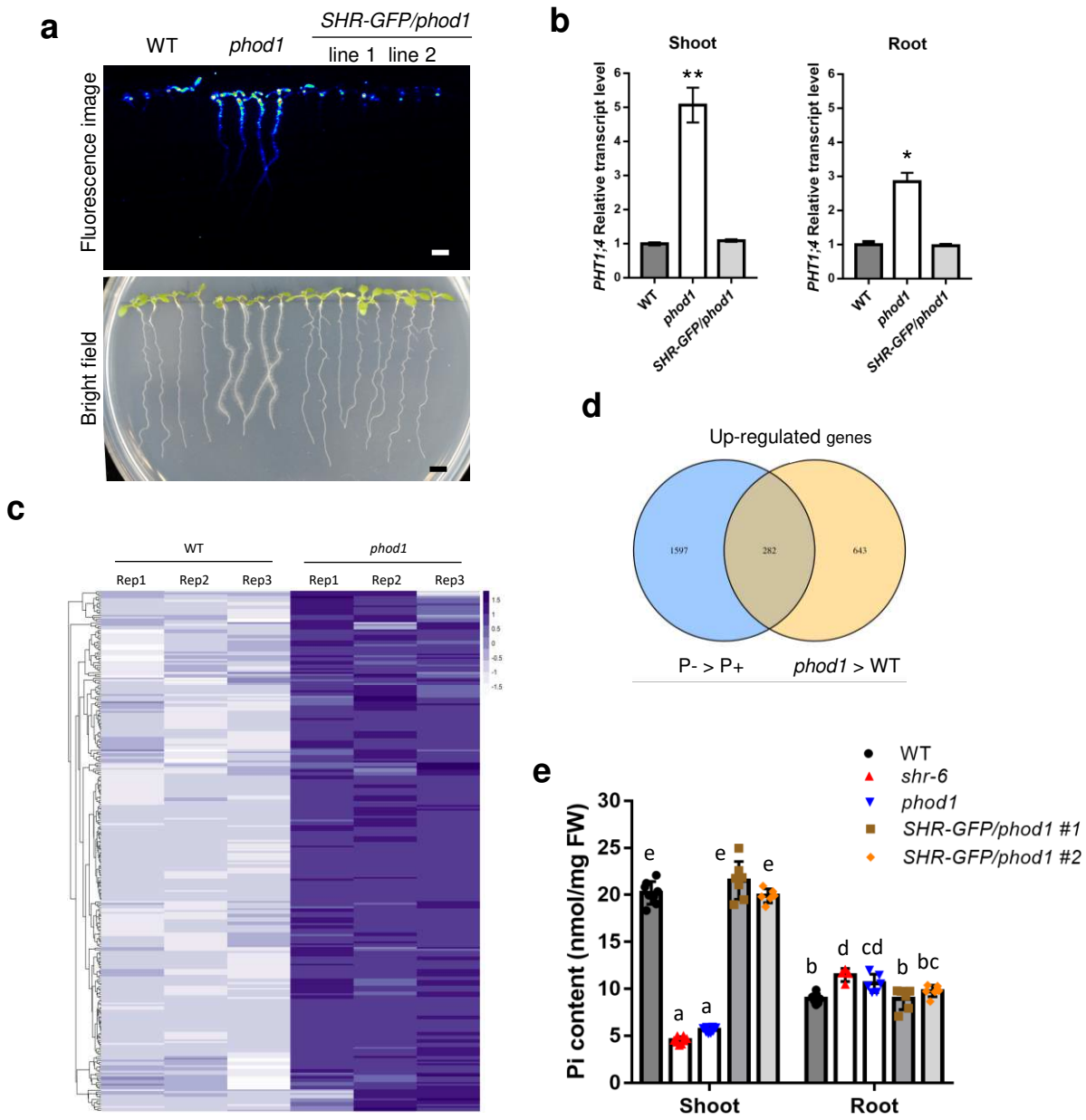

Fig. 1. SHR is required for Pi translocation to shoot. a, Comparison of *LUC* expression driven by *pPHT1;4* promoter (top part) on 1/2 MS medium among WT, *phod1* mutant, and *phod1* transformed with GFP-fused *SHR* driven by its native promoter. Scale bars 0.5 cm. **b**, Expression level of endogenous *PHT1;4* gene in WT, *phod1* mutant and *phod1* transformed with GFP-fused *SHR* driven by its native promoter. Error bars are mean ± s.d. Sets of data were analyzed by independent-samples T test (two-tailed), where two asterisks and one asterisk represent statistically significant difference at $p < 0.01$ and $p < 0.05$, respectively. **c**, Cluster display of transcripts of Pi starvation-induced (PSI) genes up-regulated in the shoot of *phod1* mutant. **d**, Diagram showing the number of genes up-regulated by Pi starvation and *phod1* mutation. **e**, Pi content in shoot or root of different genotypes shown in (**a**). Error bars are mean ± s.d. with four biological replicates and measured twice. Sets of data were analyzed by one-way ANOVA followed by Tukey post hoc test, where letters represent statistically significant difference at $p < 0.05$ for multiple comparisons.

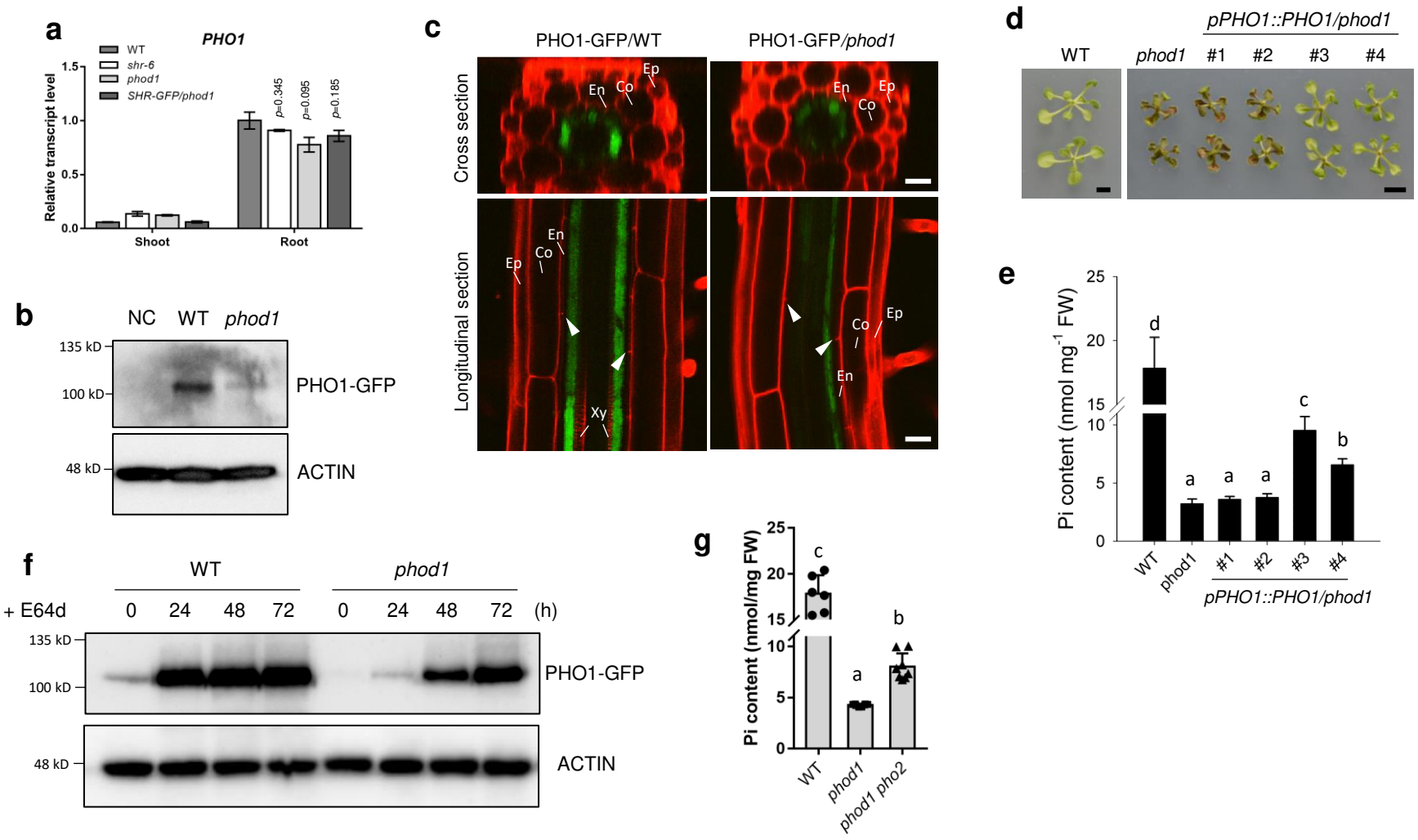

Figure 2. PHO1 localization pattern and protein levels are altered in *phod1*. **a**, Quantitative analysis of *PHO1* gene expression in the shoot and root of WT, *shr-6*, *phod1*, *SHR-GFP/pho1*. Error bars are mean ± s.d. Sets of data were analyzed by independent-samples T test (two-tailed). **b**, Western-blot analysis of PHO1-GFP protein level in the root of WT or *phod1*. NC: negative control. **c**, PHO1-GFP fusion protein fluorescence in WT or *phod1*. Green signal represents GFP fluorescence; red signal represents propidium iodide (PI) staining. The white arrow heads mark the endodermal transversal wall (the position of Casparian strip) at which PI is blocked. Ep: epidermis; Co: cortex; En: endodermis; Xy: xylem. Scale bars 20 μm. **d-e**, Morphological appearance (**d**) and Pi content (**e**) of 2-week-old WT, *phod1*, and transgenic lines with different expression level of *PHO1*. Scale bars 0.5 cm (**d**). Error bars are mean ± s.d. with three biological replicates. Sets of data were analyzed by one-way ANOVA followed by Tukey post hoc test, where letters represent statistically significant difference at $p < 0.05$ for multiple comparisons (**e**). **f**, Western blot analysis of PHO1 in root of WT or *phod1* after E64d treatment. 4-day-old seedlings were treated with E64d for three consecutive days. Roots were collected for total protein extraction and western-blot analysis. **g**, Pi content in the shoot of 9-day-old seedlings of WT, *phod1* and *phod1 pho2* double mutant. Error bars are mean ± s.d. with three biological replicates and measured twice. Sets of data were analyzed by one-way ANOVA followed by Tukey post hoc test, where letters represent statistically significant difference at $p < 0.05$ for multiple comparisons.

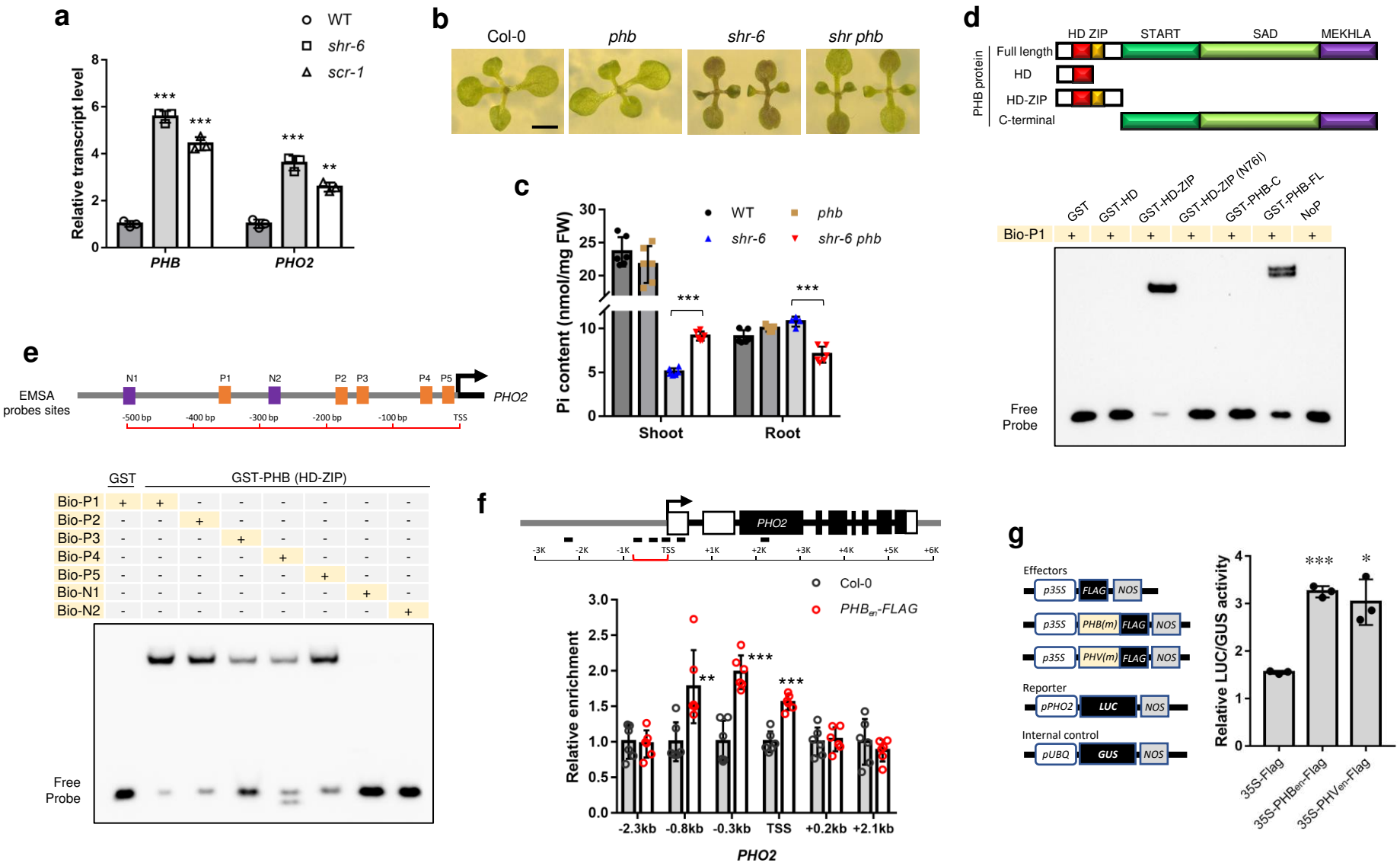

Figure 3. PHB directly regulates *PHO2* expression. a, Quantitative analysis of *PHB* and *PHO2* gene expression in the root of Col-0, *shr-6* and *scr-1* on Pi-sufficient conditions. Error bars are mean ± s.d. The bar graph shows results from three biological replicates. Sets of data were compared by independent-samples T test (two-tailed), where three asterisks and two asterisks represent statistically significant difference at $p < 0.001$ and $p < 0.01$, respectively, compared to WT. **b**, Anthocyanin phenotype in the leaves of Col-0, *phb*, *shr-6*, and the *shr-6 phb* double mutant. **c**, Pi content in the shoot or the root of different genotypes in (**b**). The bar graph shows results from 2-3 biological replicates and measured twice. Sets of data were compared by independent-samples T test (two-tailed), where three asterisks represent statistically significant difference at $p < 0.001$. **d**, Electrophoretic mobility shift assay (EMSA) of full-length and truncated PHB protein binding to P1 motif of *PHO2* promoter. Bio: biotin; FL: full-length. **e**, EMSA of HD-ZIP domain of PHB binding to different motifs in *PHO2* promoter. N1 and N2 probes acted as negative controls. **f**, Enrichment of PHB protein on *PHO2* promoter in positions shown in red in the schematic diagram. Col-0 acts as a control. TSS: transcription start site. Error bars are mean ± s.d. with two biological replicates and measurements were repeated thrice. Sets of data were analyzed by independent-samples T test (two-tailed), where three asterisks and two asterisks represent statistically significant difference at $p < 0.001$ and $p < 0.01$ compared to control. **g**, Transient expression of enhanced PHB or PHV activates the transcription driven by *PHO2* promoter in root protoplast. *pUBQ-GUS* acts as an internal control. Error bars are mean ± s.d. with three biological replicates. The three asterisks and one asterisk represent statistically significant difference at $p < 0.001$ and $p < 0.05$, respectively, compared to control analyzed by independent-samples T test (two-tailed).

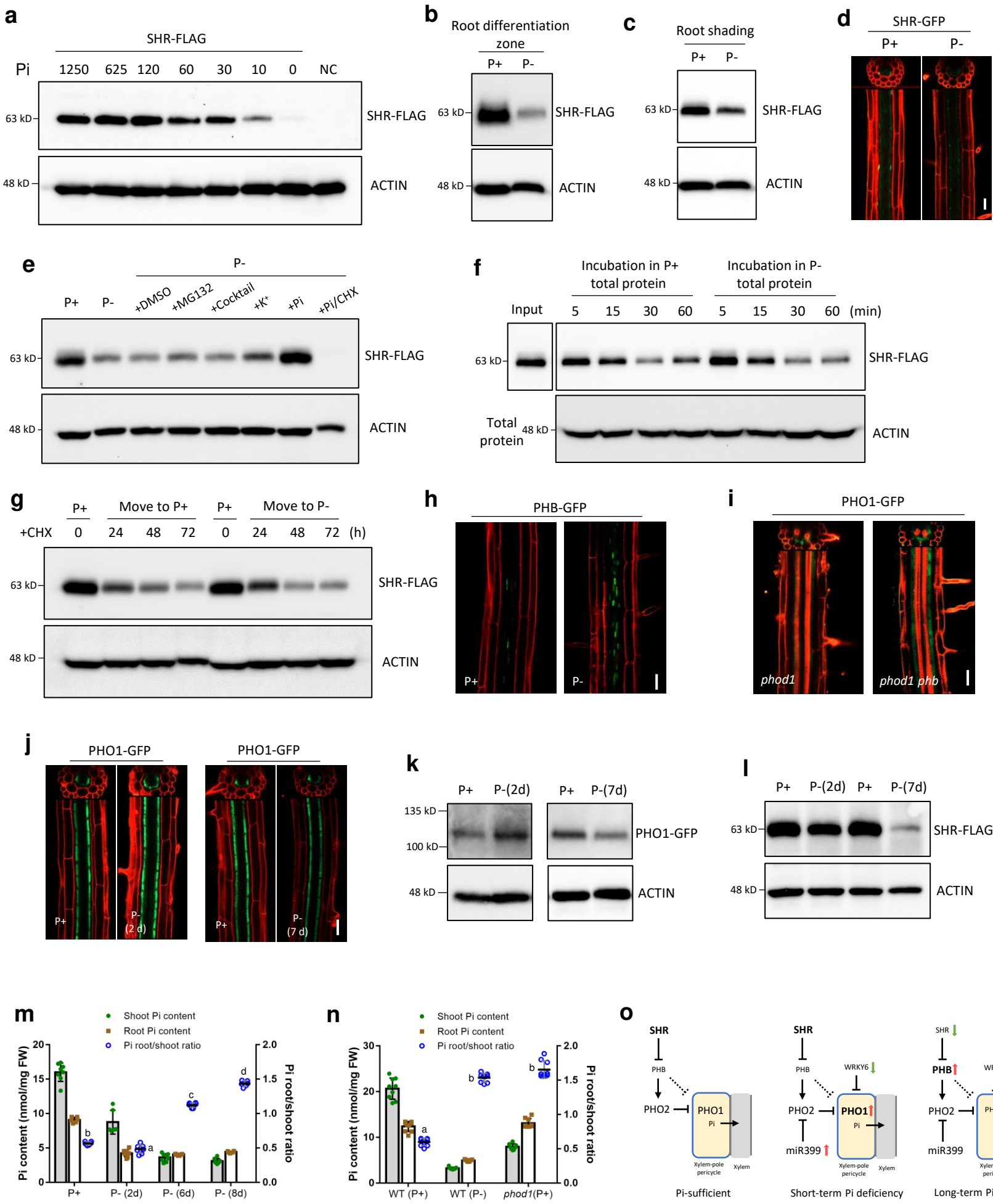

Figure 4. Decrease in SHR level in root restricts Pi allocation to shoot under long-term Pi starvation. a, Protein level of SHR in root of transgenic line under different Pi concentrations. ACTIN protein acts as the loading control. **b**, SHR protein level in root differentiation zone under Pi-sufficient (P+) or Pi-deficient (P-) conditions. **c**, SHR protein level in root under shading under P+ or P- conditions. **d**, GFP-fused SHR fluorescence indicates the localization and protein level of SHR in root differentiation zone under P+ or P- conditions with root shading. Scale bars 40 μm. **e**, SHR protein level on adding protease inhibitors, K^+ or Pi under P- conditions for 2 days. The components of Cocktail include protease inhibitors AEBSF, Aprotinin, Bestatin, E-64, Leupeptin and Pepstatin A. Pi was added in the form of 1.25 mM KH_2PO_4. **f**, Degradation of SHR protein *in vitro* by incubating equivalent amounts of total protein obtained from P+ or P- seedlings sampled at various timepoints. **g**, SHR protein level when seedlings are moved from P+ to P+ or P+ to P- conditions by adding protein translation inhibitor CHX for three consecutive days. **h**, GFP-fused PHB fluorescence indicates PHB protein level under P+ or P- conditions. Scale bar 20 μm. **i**, PHO1-GFP green fluorescence in root differentiation zone of *phod1* or *phod1 phb* double mutant (*PHB* knock-out). Scale bar 20 μm. **j**, GFP-fused PHO1 protein abundance indicated by green fluorescence in root differentiation zone under short-term (2 days) or long-term (7 days) Pi deficiency conditions. Scale bar 20 μm. **k**, Western-blot analysis of PHO1 protein level in root treated with short-term (2 days) or long-term (7 days) Pi deficiency condition. **l**, Protein level of SHR in root of 9-days seedlings suffer from short-term or long-term Pi deficiency. **m**, Pi content and its root/shoot ratio for WT plants treated by short-term or long-term Pi deficiency. Error bars are mean ± s.d. with three or four biological replicates and measurements were repeated twice. Sets of data were analyzed by one-way ANOVA followed by Tukey post hoc test where letters represent statistically significant difference at $p < 0.05$ for multiple comparisons. **n**, Decrease in SHR level elevates the root/shoot Pi content ratio in WT plants under P- condition, or in *phod1* on P+ condition for long-term (9 days). Error bars are mean ± s.d. with three biological replicates and measured thrice. Sets of data were analyzed by one-way ANOVA followed by Tukey post hoc test where letters represent statistically significant difference at $p < 0.05$ for multiple comparisons. **o**, A model for SHR regulating Pi translocation between root and shoot. Under Pi-sufficient condition, SHR is required to maintain PHO1 expression in root xylem-pole pericycle and support Pi translocation to shoot. During the early stages of Pi deficiency, PHO1 protein is enhanced in root by transcriptional and post-transcriptional regulators. However, long-term or serious Pi deficiency post-transcriptionally inhibits SHR and PHB increases in the root stele. PHO1 is suppressed by PHO2 and/or other factors. Therefore, a limited amount of Pi is locked in the root which is essential for root vitality and root expansion to forage more Pi under scarcity or in soils with heterogeneous distribution of Pi.

Supplementary Files

This is a list of supplementary files associated with this preprint. Click to download.

- Supplementarymovie1b.avi
- SHRsuplementalfigures.pdf
- Supplementarymovie2a.avi
- Supplementarymovie1a.avi
- SupplementaryTable1.xlsx
- SupplementaryDataSet1.xlsx
- Supplementarymovie2b.avi